AIAA 2013-2738

Boundary-Layer Transition Experiments in a Hypersonic Quiet Wind Tunnel

Christopher A. C. Ward*, Roger R. Greenwood*,
Andrew D. Abney*, and Steven P. Schneider†
School of Aeronautics and Astronautics
Purdue University
West Lafayette, IN 47907-1282

This paper reports the progress of three projects in the Boeing/AFOSR Mach-6 quiet tunnel at Purdue University. The first project used a 7-deg half-angle cone at 6-deg angle-of-attack with temperature-sensitive paint applied to the frustum and small roughness dots added near the nosetip. Depending on the spacing of the roughness, the spacing and breakdown of the stationary vortices was altered. The second project looked at modifications to a pulsed jet perturber to reduce the perturbation duration. This was accomplished through both electronic and physical modifications to the perturber system. Shorter duration perturbations were achieved, but further progress is required. The third project measured low-frequency disturbances in the first-mode instability frequency range with Kulite pressure transducers on the surface of a cone-ogive-cylinder model. Initial measurements show that the magnitude of the low-frequency disturbance on the cone-ogive-cylinder is greatest outside the boundary layer, which may indicate an entropy-layer instability.

Nomenclature

f	frequency	t	time
M	Mach number	x	model axial coordinate
p	pressure (psia)	y	spanwise coordinate
$\dot{q}$	heat flux	z	tunnel axial coordinate
Re	Reynolds number		
T	Temperature		

Subscripts		*Abbreviations*	
0	stagnation condition	BAM6QT	Boeing/AFOSR Mach-6 Quiet Tunnel
w	wall condition	TSP	Temperature-Sensitive Paint

I. Introduction

A. Hypersonic Boundary-Layer Transition

Hypersonic transition is important for prediction and control of heat transfer, skin friction, separation and other boundary-layer properties. Vehicles that spend extended periods at hypersonic speeds may be

*Research Assistant. Student Member, AIAA
†Professor. Associate Fellow, AIAA

critically affected by uncertainties in transition prediction. However, the mechanisms leading to transition are still poorly understood, even in low-noise environments. Boundary-layer transition is a complicated process. Disturbances can be created in the freestream (acoustic radiation or vorticity) or by the vehicular surface (surface roughness or waviness).[1] The disturbances enter the boundary layer through the process of receptivity.[2] Receptivity can be affected by roughness, bluntness, Mach number and other factors. These disturbances grow and may lead to turbulence, depending on the instabilities present in the boundary layer. Empirical or semi-empirical methods can be used to predict the growth of the instabilities and predict transition,[3] but these methods are not necessarily reliable for a wide range of cases. A more basic understanding of the flow physics that causes transition is needed, thereby reducing empiricism.

B. The Boeing/AFOSR Mach-6 Quiet Tunnel

The Boeing/AFOSR Mach-6 Quiet Tunnel (BAM6QT), shown in Figure 1, is the largest operational hypersonic quiet tunnel in the world. The BAM6QT is a Ludwieg tube, consisting of a long driver tube with a converging-diverging nozzle at the downstream end. A Ludwieg tube design was chosen since it can provide high quiet Reynolds numbers while minimizing costs. The tunnel is operated by bringing the driver tube and the test section to the desired stagnation pressure and the downstream end to vacuum, separated by a set of burst diaphragms. To run the tunnel the diaphragms are burst, causing a shock wave to travel downstream and an expansion fan to travel upstream. Mach-6 flow is initiated after the expansion fan passes through the nozzle. The expansion fan reflects between the upstream end of the driver tube and the contraction, causing a quasi-static decrease in the stagnation pressure. Therefore, during any run a range of Reynolds numbers is tested.

The BAM6QT is capable of maintaining a laminar nozzle-wall boundary layer, thus producing pitot-pressure fluctuations that are less than 0.05% of the mean. The BAM6QT employs several features to achieve this low noise. A suction slot is present upstream of the throat and removes the boundary layer on the contraction wall, allowing a new undisturbed laminar boundary layer to grow on the nozzle wall. The suction slot is connected to the vacuum tank through a fast valve. The fast valve can be closed to allow a turbulent nozzle-wall boundary layer to develop. The noise levels with a turbulent nozzle-wall boundary layer are on the order of 3%, similar to conventional hypersonic tunnels. The tunnel also features a long nozzle to damp the effect of the Goertler instability, a highly polished throat and nozzle, and high-quality air filters to reduce airborne particulate.

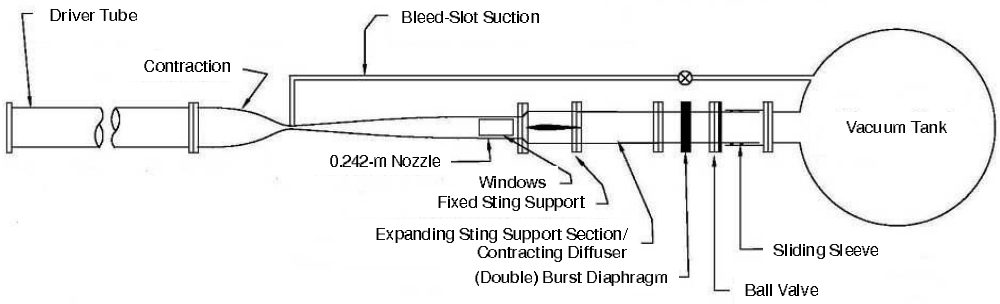

Figure 1. Schematic of Boeing/AFOSR Mach-6 Quiet Tunnel

II. Crossflow Instability and Transition on a Cone at Angle of Attack

There are several instabilities that can cause transition in a three-dimensional boundary layer, including the centrifugal, streamwise, and crossflow instabilities. For an axisymmetric cone in hypersonic flow pitched at an angle of attack, a circumferential pressure gradient is created due to a stronger shock near the windward

ray. The circumferential pressure gradient causes the inviscid streamlines to be curved. In the boundary layer, there is an imbalance between the pressure gradient and the centripetal acceleration because the streamwise velocity is reduced near the wall, but the pressure gradient does not change. This imbalance causes a secondary flow (crossflow) in the boundary layer perpendicular to the inviscid streamlines. Crossflow must vanish at the wall and the edge of the boundary layer, creating an inflection point in the crossflow velocity profile.[4] Crossflow is thus inviscidly unstable and manifests as co-rotating vortices centered around the inflection point. Crossflow waves can be either travelling or stationary with respect to the surface. It has been verified experimentally for low speeds that the stationary waves tend to dominate in low-disturbance environments such as in flight or in low-noise tunnels, while the travelling waves tend to dominate in high-disturbance environments such as conventional tunnels.[5] The stationary waves appear to be sensitive to small roughness placed near the wave's neutral point. Both Saric et al. (at low speeds) and Corke et al. (at supersonic speeds) have had much success in using discrete roughness elements to control the stationary vortices.[4,6–8] Depending on the spacing of the roughness, certain stationary vortex wavelengths could be forced, and crossflow-induced transition could delayed.

A. Results

Tests were performed in January 2013 to obtain global heat transfer from the temperature-sensitive paint on a 7° half-angle cone at 6° angle of attack. TSP is calibrated to heat transfer using a Schmidt-Boelter heat transfer gauge. A more detailed description of the calibration method is given in Reference 9. Discrete roughness elements were placed around the azimuth, 2.0 inches from the nosetip, near the neutral point of the most unstable stationary modes according to calculations by Li et al.[10] The discrete roughness elements were created by pressing a conical stainless steel rod into a Torlon section of the cone, similar to the roughness elements used by Schuele.[8] Three different Torlon sections were manufactured, one with no dimples, one with 50 dimples (spaced 7.2° apart), and one with 72 dimples (spaced 5° apart). The roughness elements had an approximate depth of 30 μm, a height of 10 μm and a diameter of 300 μm. Preliminary results with the roughness elements were shown in Reference 11.

To determine if the stationary vortices are being created by the roughness elements, the cone was rotated approximately 10°. If the stationary vortices roll with the cone, then they are body fixed. The 50-dot case is shown in Figure 2. Spanwise heat transfer profiles taken at an axial distance of 0.35 m are plotted. 0° corresponds to the leeward ray. For the 50-dot case, the peaks and valleys of the stationary waves show good agreement with each other. The discrepancies in heat transfer between the two tests are likely caused by slightly different tunnel conditions or model wall temperatures.

The 72-dot case was also examined to determine if the stationary vortices are body fixed. Spanwise heat transfer is plotted in Figure 3. The peaks and valleys of the stationary vortices appear to agree fairly well with each other, but there is some discrepancy near 15–25° from the lee ray. The cause of this discrepancy is not known. Comparing the 50 and 72-dot case, there is a different pattern of stationary vortices being generated. Therefore from these tests, the dimples near the nosetip appear to be generating stationary vortices.

Additional experiments were performed in May 2013 with the leading edge of the paint moved much further downstream on the cone. In previous experiments, the paint would begin approximately 3 inches from the nosetip. For the experiments shown below, the paint began at approximately 13 inches from the nosetip, as suggested by Dr. Meelan Choudhari of NASA Langley. This was done to minimize the effect the paint edge and the painted surface has on the generation of the stationary vortices (by moving the paint much further downstream of the neutral point of the most amplified stationary waves). The paint edge had a slope of 10 μm/mm. The painted surface had an RMS roughness of 0.16 μm, and the machined-finished surface of the cone had an RMS roughness of 0.07 μm.

TSP images with no roughness, 50 roughness dots and 72 roughness dots around the azimuth are shown in Figure 4 at a Reynolds number of approximately 10.5×10^6/m. It appears that each case is producing a different spacing of the stationary vortices. As was seen in previous experiments,[11] it appears that the stationary vortices are breaking down near the lee ray for the smooth and 72-dot case. The vortices do not appear to break down for the 50-dot case. Spanwise heat-transfer profiles are taken for the three cases at

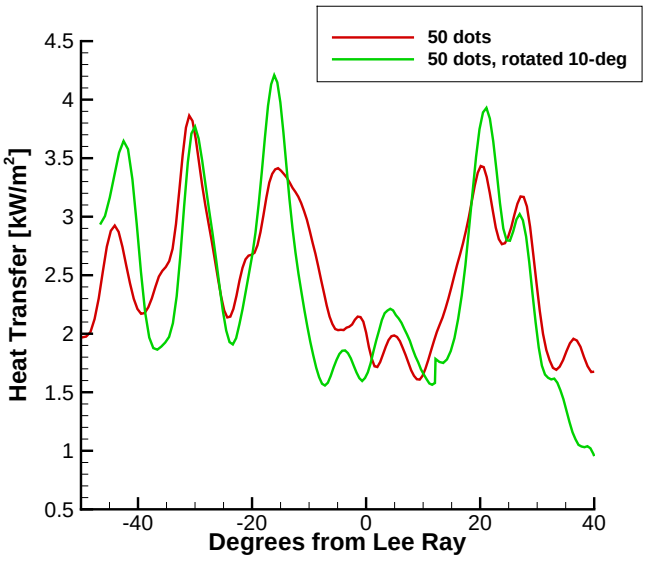

Figure 2. Spanwise heat transfer profiles at an axial distance of 0.35 m. 50-dots case. Approximate conditions of Re = 10.7×10^6/m, p_0 = 149 psia, T_0 = 423 K.

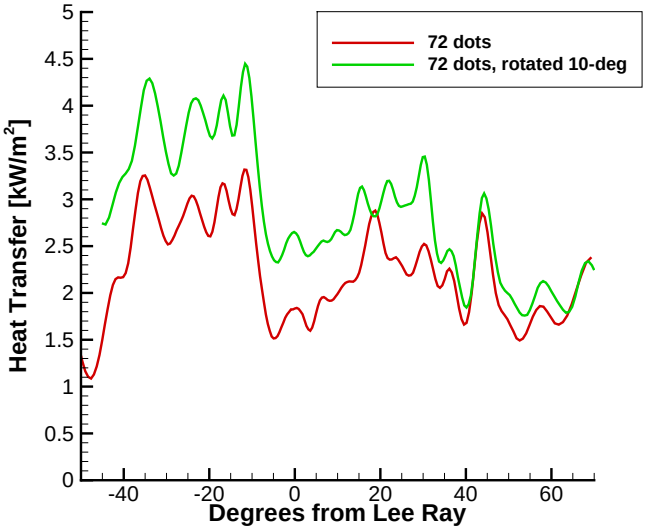

Figure 3. Spanwise heat transfer profiles at an axial distance of 0.35 m. 72-dots case. Approximate conditions of Re = 10.5×10^6/m, p_0 = 149 psia, T_0 = 427 K.

an axial location of 0.35 m, and are shown in Figure 5. From this plot, an approximate wavenumber can be determined (number of vortices per circumference of the cone). For the 72-dot case the wavenumber is approximately 68, close to the expected value. For the 50-dot case the wavenumber is approximately 44, also close to the expected value. The smooth case produces an approximate wavenumber of 54. It can be seen

more clearly here that the three different roughness cases are generating different spacing of the stationary vortices.

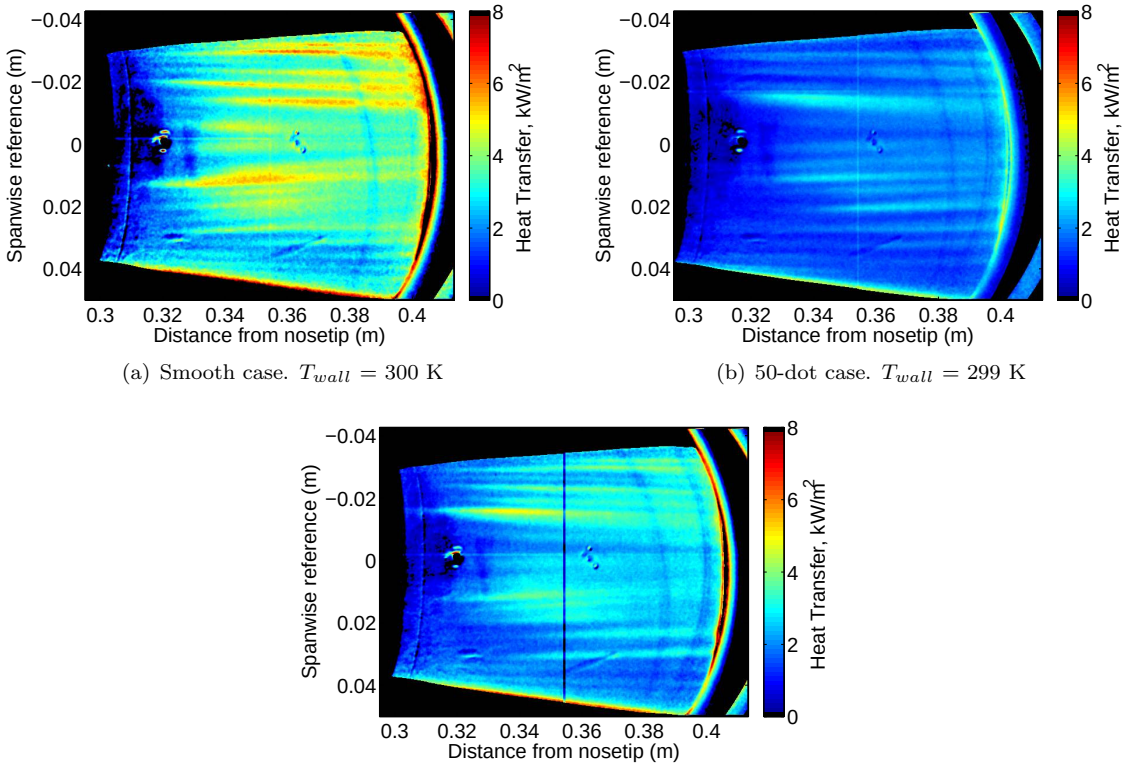

(a) Smooth case. $T_{wall} = 300$ K

(b) 50-dot case. $T_{wall} = 299$ K

(c) 72-dot case. $T_{wall} = 299$ K

Figure 4. TSP images of the 7° half-angle cone at 6°. Lee side of the cone. Quiet flow. Paint edge 13-inches from the nosetip. $p_0 = 136$ **psia, Re** $= 10.5\times10^6$**/m,** $T_0 = 425$ **K**

The data with the paint edge beginning 13 inches from the nosetip can be compared to data with the paint edge beginning approximately 3 inches from the nosetip. The data with the paint edge beginning 3 inches from the nosetip was presented in Reference 11, and is shown below in Figure 6. Clearly there is a difference in the stationary vortices comparing the TSP images in Figure 6 to the TSP images in Figure 4. The difference can be seen more clearly in Figure 7, which shows spanwise heat transfer profiles at an axial distance of 0.35 m with the paint edge 3 and 13 inches from the nosetip. It appears that although that the step at the leading edge of the paint is small, it is still having a significant effect on the generation of the stationary vortices. All three cases create much different patterns of stationary vortices with the paint edge moved much further downstream. Therefore future tests should have the paint edge as far downstream as possible to reduce the effect of the paint edge and the painted surface on the generation of the stationary vortices. Nonetheless, the new data shows that the applied roughness elements may be dominating the generation of the vortices. This result is crucial, as now the important geometrical parameters of the roughness elements and their effect on the stationary vortices can be identified. Future work will begin to look at the effect of larger and smaller roughness (2-inches from the nosetip) on the generation and breakdown of the stationary vortices.

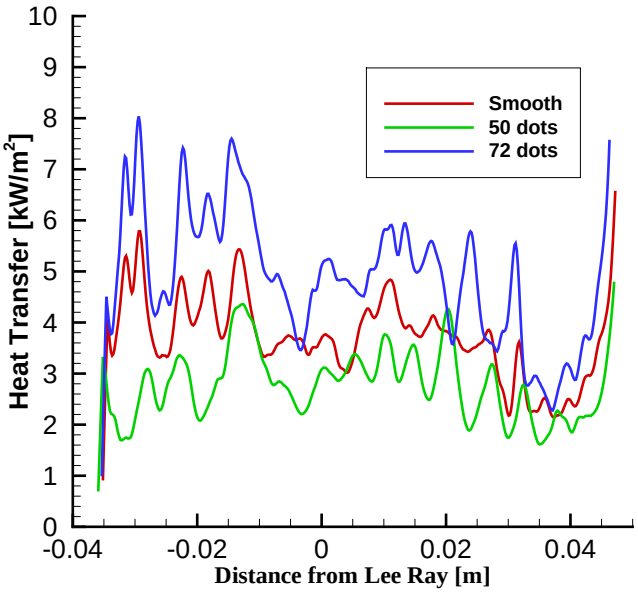

Figure 5. Spanwise heat transfer profiles of TSP images in Figure 4 at an axial distance of 0.35 m.

III. Measurements of Low-Frequency Instabilities on a Cone-Ogive-Cylinder in the Boeing/AFOSR Mach-6 Quiet Tunnel

A. Introduction

Much of the hypersonic regime is dominated by fast-growing second-mode instabilities. A method for measuring the second-mode instability with robust surface transducers has been used successfully in various conventional and quiet hypersonic tunnels.[12,13] However, blunt vehicles and other configurations where the edge Mach number is lower are also susceptible to first-mode instabilities. One recent example of a first-mode-dominant design is the entry vehicle for the Mars Science Laboratory. Computations of the vehicle design showed the dominance of first-mode instabilities and correlated them to transition measurements from ground tests. However, actual experimental measurements of the first-mode instabilities were not made.[14]

Experimental measurements of first-mode instabilities are limited, fairly inconclusive, and have predominantly used fragile sensors, such as hot-wire anemometers.[15–22] Recent measurements on a cone at angle of attack in the Mach-6 tunnel at Braunschweig provide showed probable first-mode instabilities using robust sensors.[23] However, an axisymmetric design is necessary to develop a process of designing for and measuring the first-mode instability in multiple tunnels. Three-dimensional computational analysis would make the process much too challenging for broad implementation.

An additional characteristic of blunt models is the entropy layer created by the shock curvature. Experimental measurements of entropy-layer instabilities are very limited. Little is understood about these instabilities and the effect they may have on boundary-layer transition. In one report, Stetson et al. followed an entropy-layer instability by measuring the location of peak energy at each axial location from its beginning outside of the boundary layer until it was swallowed in the boundary layer. They discovered that the entropy-layer disturbances grew slowly outside the boundary layer, diminished slightly as they entered the boundary layer, and then proceeded to grow rapidly inside the boundary layer.[24] As with the first-mode instability, experimental measurements of the entropy-layer instability are required to understand the physics and to develop mechanism-based prediction methods.

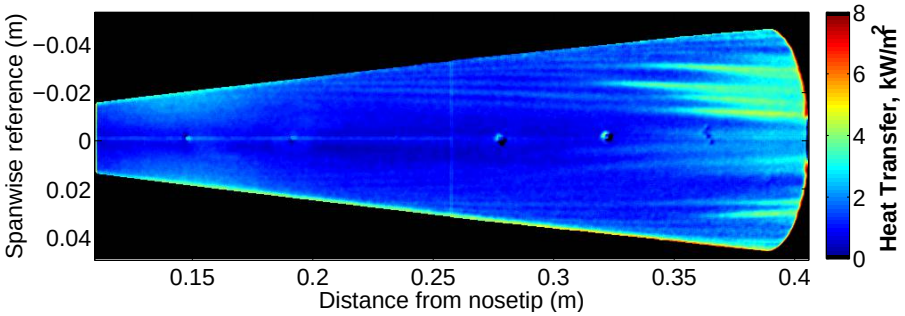

(a) Smooth. T_{wall} = 297.6 K.

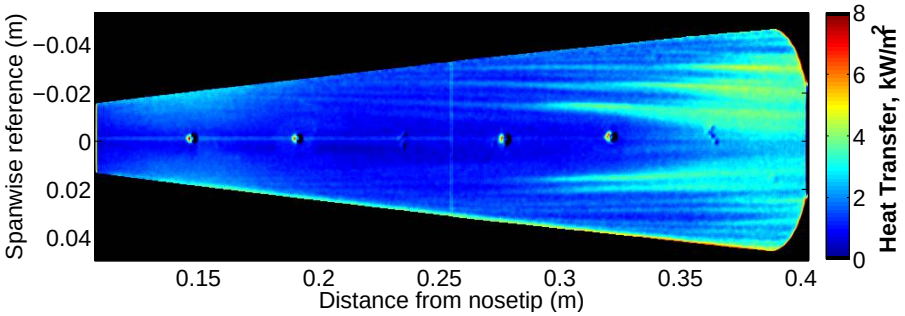

(b) 50 dots. T_{wall} = 295.3 K.

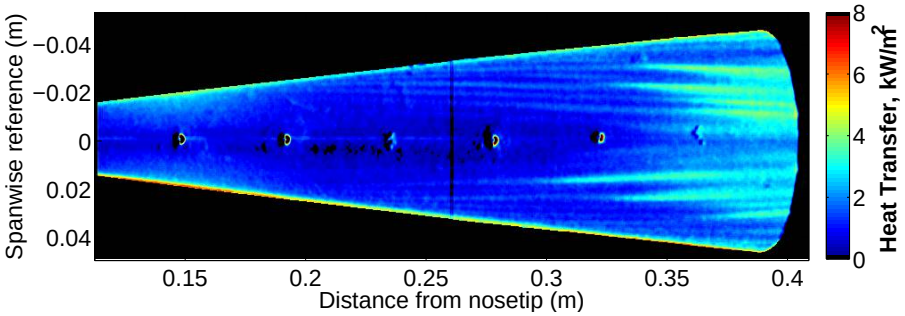

(c) 72 dots. T_{wall} = 299.7 K.

Figure 6. TSP images of 7°half-angle cone at 6°angle of attack. Lee side of the cone. Quiet flow. Paint edge 3-inches from the nosetip. Re = 10.5×10^6/m. p_0 = 138 psia. T_0 = 426 K. Data previously presented in Reference.[11]

The cone-ogive-cylinder design being used for experiments in the BAM6QT has large leading-edge angles in order to reach the low edge Mach numbers where first-mode instabilities become dominant. These large angles also result in significant shock curvature, which creates an entropy layer. A numerical analysis by Reshotko and Khan showed that instabilities within the entropy layer are similar to first-mode instabilities calculated for a supersonic boundary layer.[25] Because of the similarity of first-mode and entropy-layer instabilities, care must be taken to distinguish between the two instabilities. The power spectra of initial measurements taken on the surface of the cone-ogive-cylinder in the BAM6QT showed disturbances in the predicted first-mode instability range, but these disturbances did not show all the expected characteristics of a first-mode instability. Off-surface measurements were made using a pitot probe to determine the identity of the disturbance.

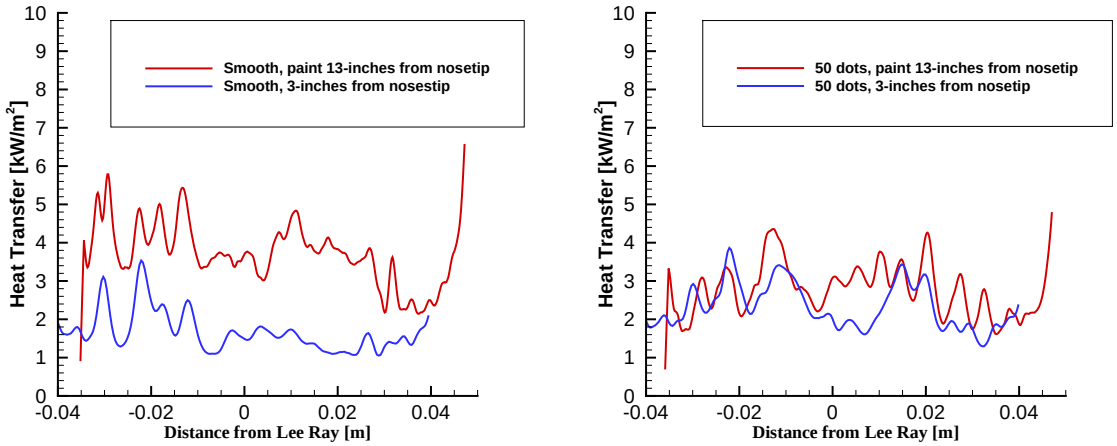

(a) Smooth case.

(b) 50-dot case.

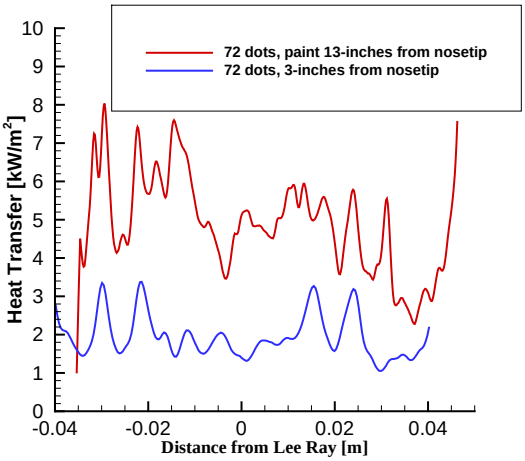

(c) 72-dot case.

Figure 7. Spanwise heat transfer profiles of TSP images in Figure 4 and 6 at an axial distance of 0.35 m.

B. Computational Setup

Mean flow and stability calculations were performed on a series of geometric configurations in an effort to find the design that would provide the best opportunity to measure first-mode instability waves in the BAM6QT.[11] The mean flow was calculated under BAM6QT operating conditions using Stability and Transition Analysis for Hypersonic Boundary Layers (STABL). STABL is a two-dimensional/axisymmetric, Navier-Stokes solver developed at the University of Minnesota that uses implicit Data-Parallel Line Relaxation (DPLR). The stability analysis was completed using PSE-Chem which solves the parabolized stability equations and predicts the N factor for each instability mode in the boundary layer.[26,27]

C. Computational Results

One of the axisymmetric geometries designed was a cone-ogive-cylinder as shown in Figure 8. This design consists of a large leading-edge half-cone angle which decreases the edge Mach to just below Mach 5, at which

point the stability analysis shows the first-mode instability becomes more amplified than the second-mode instability. The half-cone angle required for this to happen in the BAM6QT is between 25 and 30 degrees.

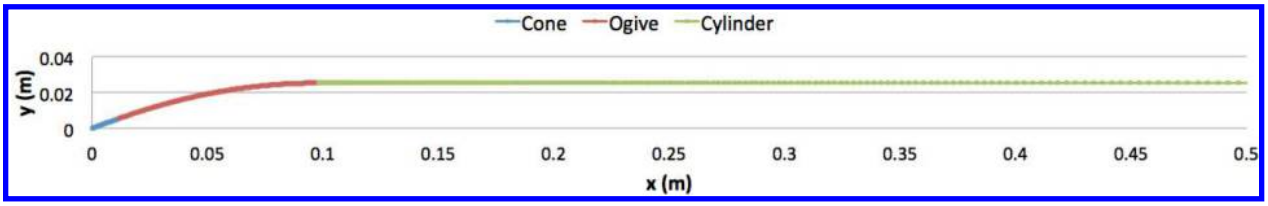

Figure 8. Cone-Ogive-Cylinder geometry.

Figure 9 shows the stability results for the cone-ogive-cylinder with a 30-degree nosetip under BAM6QT conditions with a total pressure of 160 psia. Under these conditions, the maximum first-mode N factor, shown as the black dot-dashed line, is predicted to be about 3 at 0.6 meters downstream. The predicted frequency and wave angle at this location are about 17 kHz and 69 degrees respectively. At this same location, the maximum second-mode N factor is about 2. As the operating pressure decreases to 80 psi, the predicted maximum first-mode N factor decreases to about 1.5 at a frequency of about 10 kHz. Previous experimental second-mode instability measurements have been made in a conventional tunnel at predicted N factors as low as 2.3.[28]

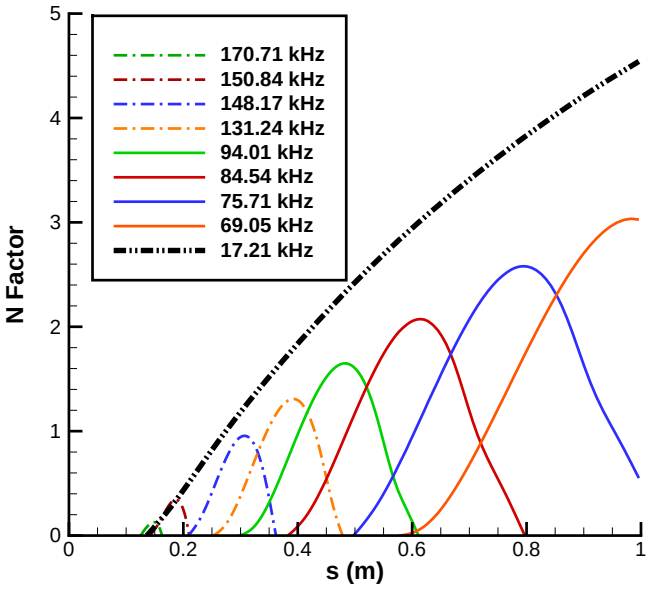

Figure 9. Stability Results for the cone-ogive-cylinder geometry under BAM6QT conditions at 160 psi.

D. Experimental Setup

The cone-ogive-cylinder design was constructed in the AAE department machine shop. The nosetips were made of stainless steel and the afterbody was made of 6061-T6 aluminum. The model is 1-meter long with a 5-cm diameter. This model is shown with a 30-degree half-angle nosetip in Figure 10.

The sketch in Figure 11 shows the pressure transducer port locations for inserting Kulite XCQ-062-15A

Figure 10. Picture of the cone-ogive-cylinder with the 30-degree nosetip.

pressure transducers that have a resonant frequency of about 300 kHz. The ports have been machined in the cone-ogive-cylinder at axial locations of 0.58, 0.61, 0.71, 0.81, and 0.91 meters. One additional port was machined on each side of the 0.61-meter location at 0.25 centimeters from the original port, measured from the port centers. Three interchangeable nosetips have been built for this model with leading-edge half angles of 28, 30, and 33 degrees. These nosetips are shown in Figure 12.

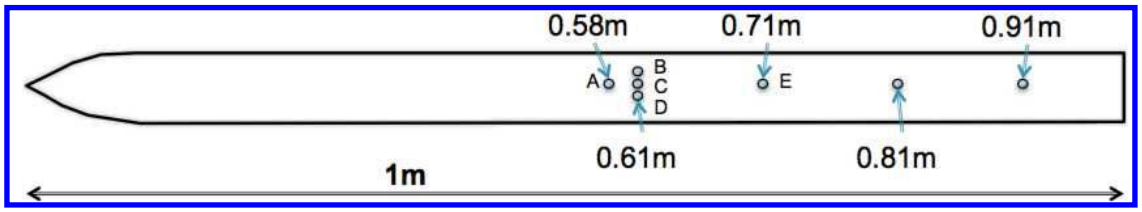

Figure 11. Sketch of the cone-ogive-cylinder with sensor locations.

Figure 12. Picture of the cone-ogive-cylinder 28°, 30°, and 33° nosetips.

Additionally, pitot probes have been used to take pressure measurements away from the surface of the model. The goal of these measurements was to determine if the amplified low frequencies from the initial experiments were first-mode or entropy-layer waves. One of the pitot probes which has been used is shown in Figure 13. Axial positioning of the pitot Kulite sensor can be made between runs, and a traversing system with a linear motor allows for vertical displacement during the run.

E. Experimental Results

Low-frequency power spectra from the flush-surface Kulite pressure transducer at 0.58 meters are shown in Figure 14. The spectra over a range of tunnel conditions show a peak at a frequency of just around 22 kHz, near the predicted maximum first-mode frequency of 17 kHz. The power spectra results obtained at 0.61 and 0.71 meters also show peaks at 22 kHz. At each location, the magnitude of the disturbance decreases as the pressure decreases. However, the frequency of the peak does not decrease as predicted for the first-mode instability.

Figure 13. Pitot Probe with installed B-screen Kulite pressure transducer.

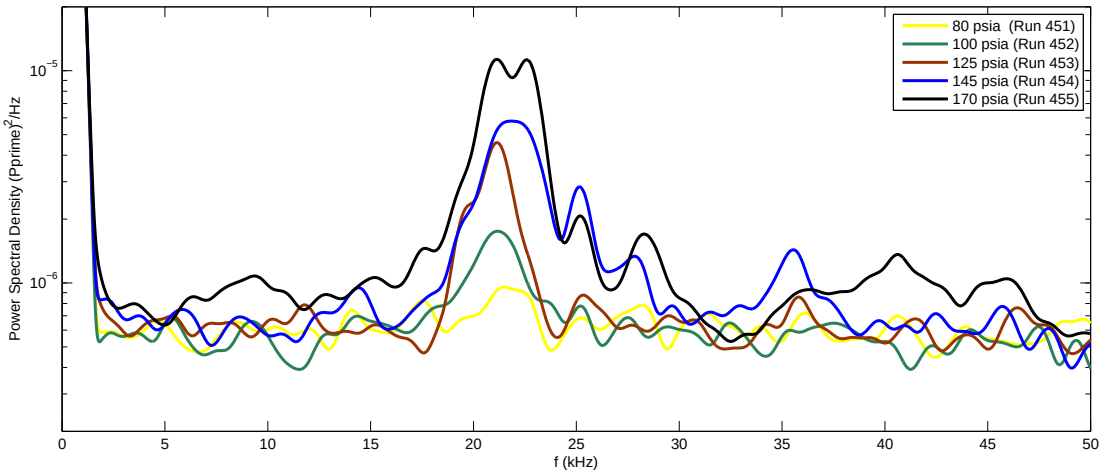

Figure 14. Power spectra showing low-frequency disturbances on the Cone-Ogive-Cylinder at 0.58 m.

To verify that the measured low-frequency disturbance was not due to model vibrations or electronic interference, one of the sensors at 0.61 meters was isolated from the flow by covering it with tape as shown in Figure 15. Figure 16 shows the resultant power spectrum for each of the sensors. The covered sensor did not measure the disturbance, indicating that the measured disturbance is not due to model vibrations. This was repeated while covering a different sensor with similar results.

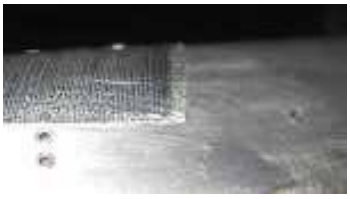

Figure 15. Tape covering one of the sensors on the Cone-Ogive-Cylinder.

Experiments were then conducted to investigate the possibility that the measured low-frequency disturbance is an entropy-layer instability. The first experiment was to place a disruption just before the array of 3 pressure sensors at 0.61 meters. It was assumed that a physical disruption of the boundary layer would produce a change in a boundary-layer instability. STABL mean-flow computations predict a boundary-layer thickness of 5 mm. However, a disruption of nearly 4 mm (shown in Figure 17) produced no significant change in the power spectra.

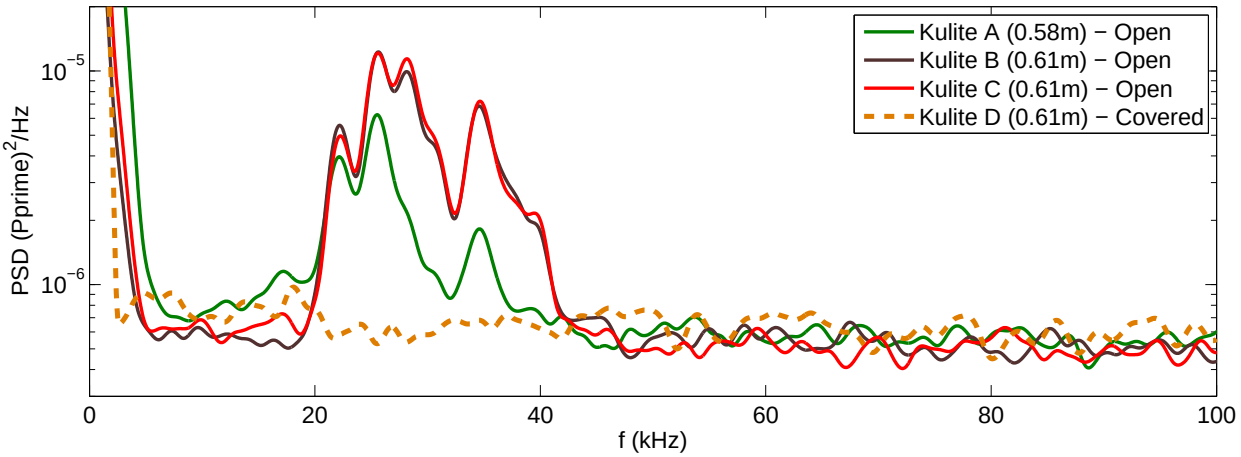

Figure 16. Power spectra showing low-frequency disturbances with one sensor (Kulite D) isolated from the flow.

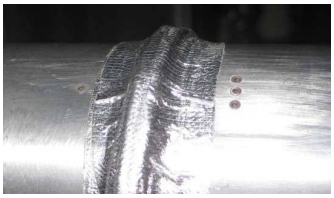

Figure 17. 4 mm disruption at on the Cone-Ogive-Cylinder at 0.6 meters.

The next experiment was to make pitot pressure measurements at several locations off the model surface to determine the radial location of the maximum disturbance. Preliminary measurements were made with a Kulite pitot probe at axial locations of 0.58 and 0.62 meters on the cone-ogive-cylinder with the 28 and 30-degree nosetips. The distance from the center of the probe to the model surface for these measurements ranged from about 2 to 26 mm. At this axial location, STABL predicts the boundary-layer thickness on the cone-ogive-cylinder to be approximately 5 mm. Spectra for these pitot measurements showed no discernible instability inside the predicted boundary layer. However, at some point outside of the boundary layer for both axial locations, and with both nosetips, the power spectra show a peak near the 22 kHz frequency detected by the surface sensors.

Figure 18(a) shows the PSD for the cone-ogive-cylinder with the 28-degree nosetip at 0.58 meters. Measurements were only made at a few locations and future measurements are planned to fill in the gaps. However, the preliminary measurements show an instability magnitude at 16 mm above the model surface that is higher than at 6 or 26 mm.

Figure 18(b) shows the spectra further downstream, at 0.62 meters. At this axial location, the maximum instability seems to be closer to the model surface as shown by the peak in the spectra for the measurement at 6 mm.

Figure 19(a) shows the PSD for the cone-ogive-cylinder with the 30-degree nosetip at 0.58 meters. The highest magnitude instability among these preliminary measurements is 20 mm. Figure 19(b) shows the spectra at 0.62 meters. As in the 28-degree nosetip case, no instabilities were identified inside the predicted boundary-layer thickness, and the spectra appears to show the instability becoming closer to the model farther downstream.

These measurements are very preliminary, but the data suggest that any instability reaches a maximum above the predicted boundary layer height. This data, and the data indicating that the maximum disturbance

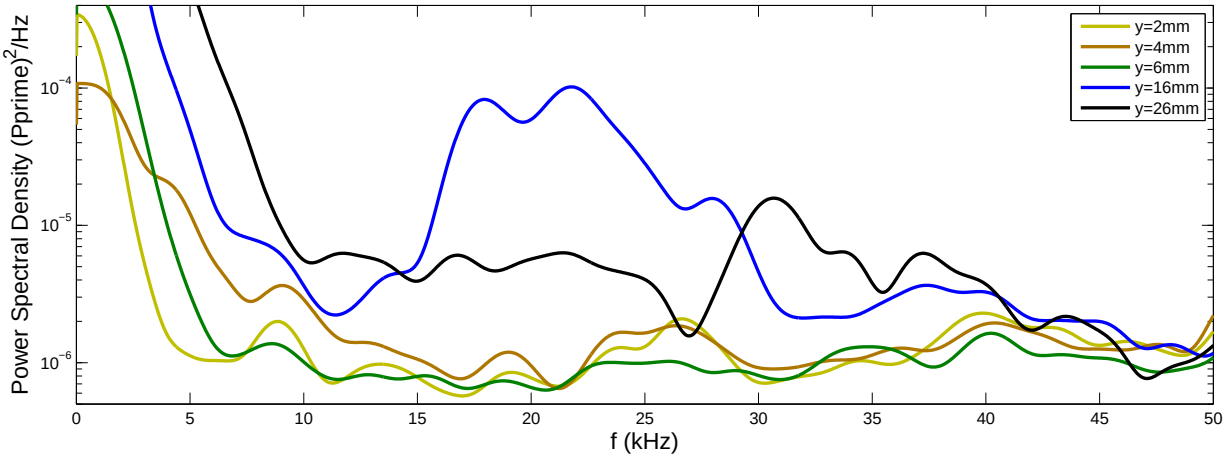

(a) PSD on pitot above the cone-ogive-cylinder with the 28-degree nosetip at an axial location of 0.58 m.

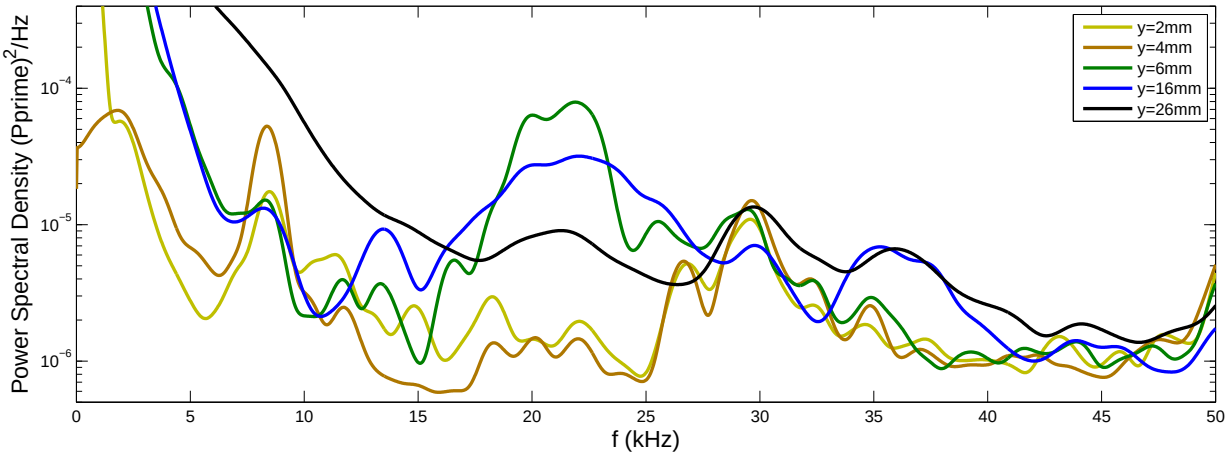

(b) PSD on pitot above the cone-ogive-cylinder with the 28-degree nosetip at an axial location of 0.62 m.

Figure 18. Pitot PSD Results at several locations above the cone-ogive-cylinder with the 28-degree nosetip.

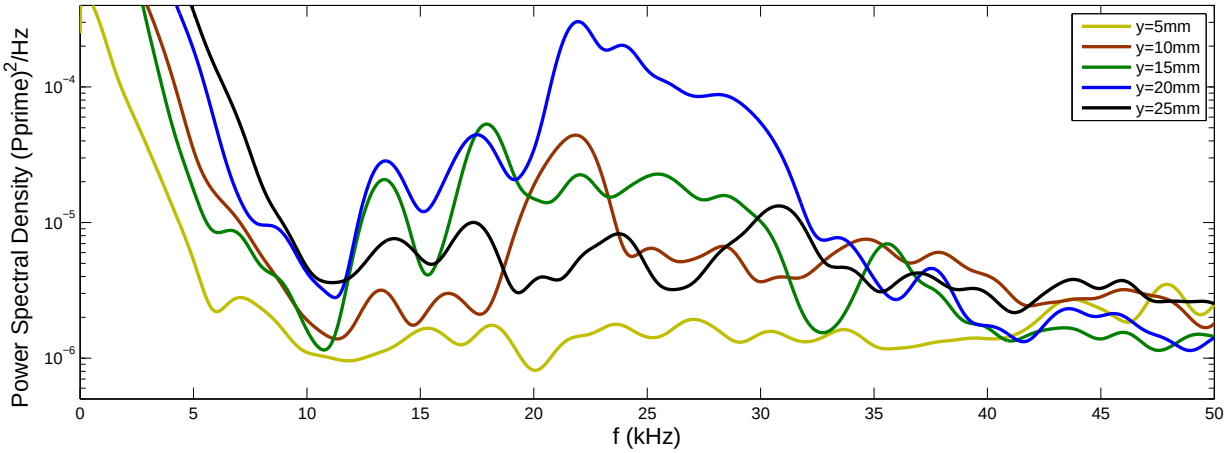

(a) PSD on pitot above the cone-ogive-cylinder with the 30-degree nosetip at an axial location of 0.58 m.

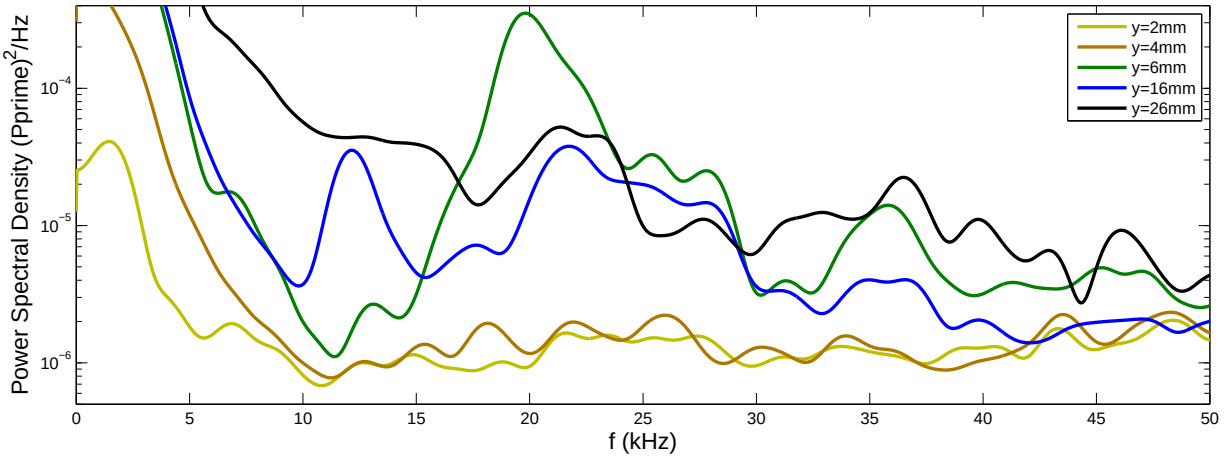

(b) PSD on pitot above the cone-ogive-cylinder with the 30-degree nosetip at an axial location of 0.62 m.

Figure 19. Pitot PSD Results at several locations above the cone-ogive-cylinder with the 30-degree nosetip.

location may be approaching the model, could be indicative of an entropy-layer instability that will eventually be swallowed up in the boundary layer. Measurements at additional axial and radial locations need to be taken to in order to better characterize and classify these low frequency disturbances. Computational comparisons to the experimental results are also needed.

IV. Towards improvement of turbulent spot generation on the nozzle wall of the BAM6QT

Transitional flow over a hypersonic vehicle produces pressure fluctuations which can impact the structural design of internal components, and has been shown to contain higher amplitude fluctuations than in fully turbulent flow. Since the transitional flow region can cover large portions of a hypersonic vehicle's body,[29] accurate modeling of the transition process and the underlying pressure fluctuations is useful for vehicle design. These fluctuations occur due to the intermittent passage of turbulent spots. Early turbulent spot models of transition assumed simple superposition of lateral merging of turbulent spots. However, Sandham's recent DNS computations of laterally merging turbulent spots in a supersonic boundary layer showed increased upwash at the merging tips, resulting in an inflectional velocity profile and production of new coherent structures.[30] Similar results were found at low speed by Makita and Nishizawa.[31] The pressure fluctuation field underneath turbulent spots is still poorly understood in a hypersonic flowfield. It is desired to combine the intermittency model of turbulent spot transition with accurate details of the pressure fluctuation environment of individual turbulent spots to better estimate pressure fluctuation levels in hypersonic flight, similar to the model developed by Park and Lauchle for low speed flat plate flows.[32]

Casper studied the pressure field of turbulent spots in a hypersonic boundary layer in the BAM6QT using a pulsed glow perturber at an axial location of z = 1.924 m from the throat.[33,34] Casper was able to measure the development of instability wave packets and their eventual transition to turbulent spots along the nozzle wall boundary layer in the BAM6QT using a streamwise array of XCQ-062-15A Kulite pressure transducers. Unfortunately, the instability waves did not transition quickly enough, and measurements of laterally merging turbulent spots could not be made within the limitations imposed by the BAM6QT nozzle design. In order to measure laterally merging turbulent spots, a pulsed jet perturber was designed, based around a Parker 009-1669-900 pulse valve.[11] The new perturber was located at the same axial location as Casper's glow perturber. The perturber successfully produced high amplitude disturbances that transitioned prior to the first measurement location at z = 2.201 m. Unfortunately, the duration was longer than desired, resulting in ambiguity as to whether the disturbances were true turbulent spots or quasi-steady-state flowfields resulting from a transverse jet. Modifications to reduce the pulse duration were developed.

A. Pulsed Jet Perturber Modifications

Modifications were made to two parts of the perturber system: the electronics that powered the valve and the poppets internal to the valve. The valve electronics are based on a design from the Jonathan Amy Facility for Chemical Instrumentation (JAFCI) at Purdue. In order to drive the valve at microsecond time scales, a short duration 300V pulse on the order of 40-100 μs is used to actuate the soleniod at high speeds. This pulse is then followed by a low voltage level (5-8 V) to hold the valve open if a longer duration is desired. The minimum duration of the low voltage signal in the stock driver electronics was 120 μs from the beginning of the driving signal. During initial testing of the perturber system, using a driver borrowed from the Zwier group in Purdue's Chemistry department, it was realized that the holding voltage duration was the limiting factor for the performance of the system. During construction of new valve driver electronics the timing circuit was modified to allow the low voltage pulse to be completely eliminated from the signal. The triggering circuit was also modified to increase the repetition rate from 50 Hz up to 180 Hz and then again to 400 Hz. The new driver circuitry had an immediate impact on the performance of the system. Figure 20 shows the performance improvements due to the modified driver, built by AAE electronic technician John Phillips. The two samples are taken at a similar freestream Reynolds number, with a valve stagnation pressure of 80 psig, using the stock polyether ether ketone (PEEK) poppets. Further tuning of the valve

driver found that an optimal high voltage pulse length was near 70 μs, but varied based on the poppet used and the adjustment of the valve.

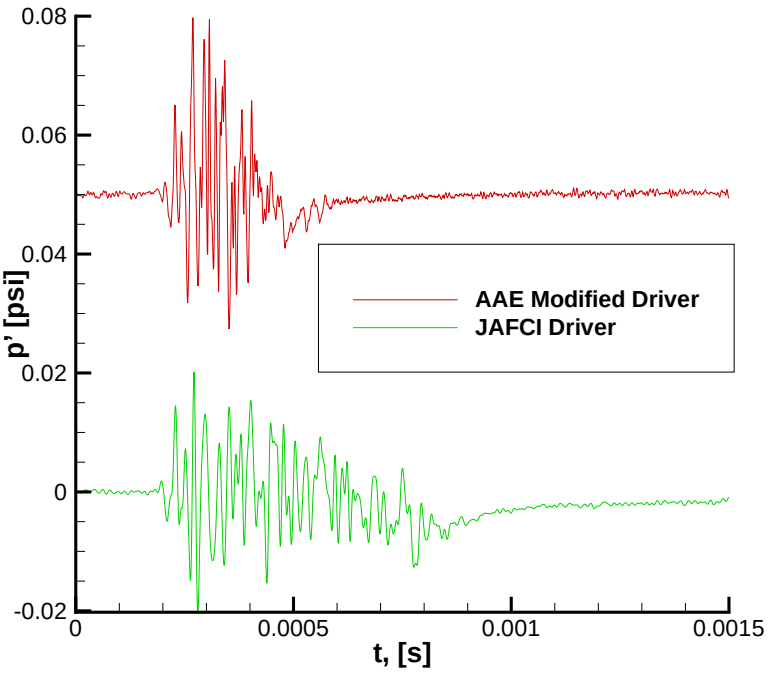

Figure 20. Performance comparison of two different drivers, uncalibrated

Additionally, the valve poppets were modified in an effort to reduce the valve-open time. Figure 21 shows the modification used, with an added 0.039 inch diameter cylindrical face. This face allowed the poppet to countersink within the body of the valve. It was hoped that the countersinking action would allow a portion of the valve travel to occur with the valve still sealed, reducing the total valve open time. The new poppets were tested with face depths between 0.003 and 0.011 inches and compared to results with a stock poppet. All of the poppets were tested at freestream unit Reynolds number of 12×10^6/m. The valve is assembled by threading the body onto the valve coil with a 1/2-28 UNEF thread. The valve is then tightened under operation until pressurized air can be felt escaping the valve under operation. At this point the valve operation is tuned by feeling for the lightest possible burst of air, at which point the valve is locked into place. This results in difficulty in aligning the valve, as an adjustment of 10° covers 20-33% of the total valve travel, and the procedure is subjective. Figure 22 shows the duration of the perturbations at z = 2.201 m as determined using a modified form of the method of Ching and LaGraff.[35] Due to the current alignment issues, it is unclear at this point whether the disturbance variation is due to the poppet modifications or valve alignment.

In order to alleviate the alignment difficulties, an alignment test bed was designed to improve the consistency of valve operation. Figure 23 shows the assembled tester sans pressure sensor. The new assembly will allow a pressure sensor readout to replace the tactile sensation test currently in use. Additionally, in an effort to reduce the time required for sufficient massflow to occur, the valve orifice area will be increased incrementally. The stock valve is rated to seal at 750 psig, which should allow for increasing the valve orifice area without a deterioration in the valve's ability to seal under tunnel pressurization.

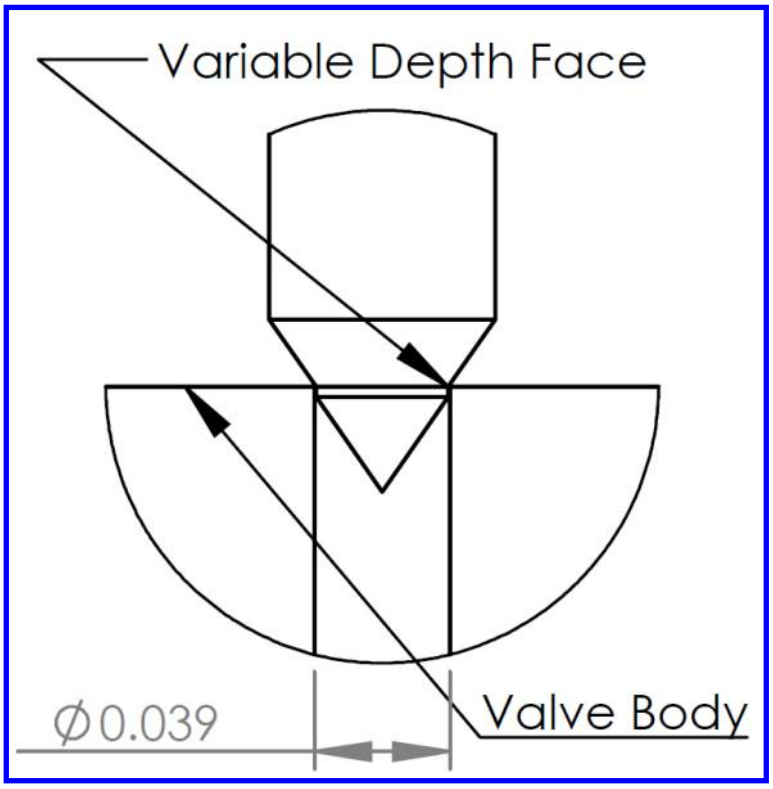

Figure 21. Schematic of poppet modification

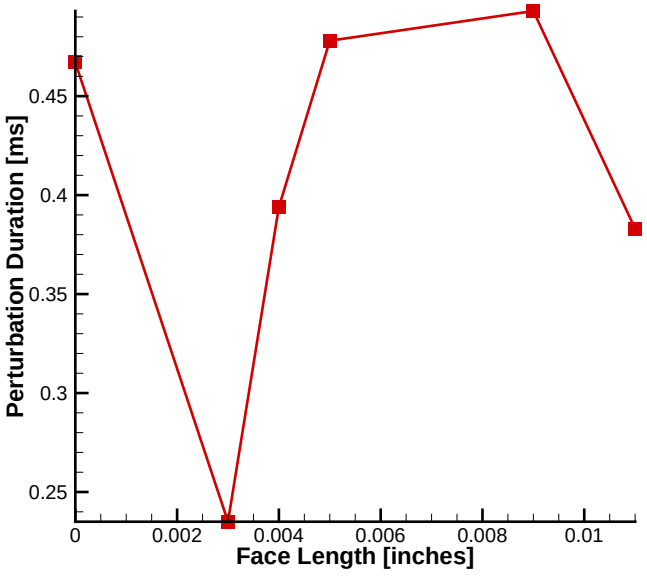

Figure 22. Disturbance duration for different poppet lengths measured at z = 2.201 m

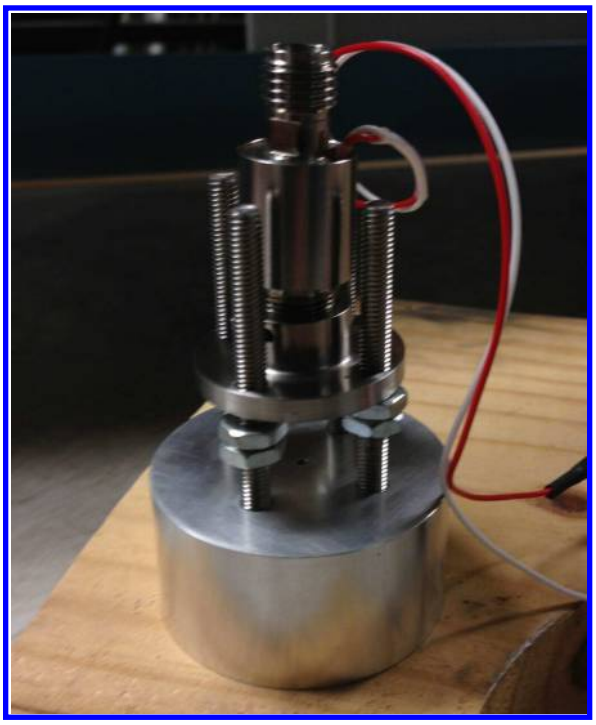

Figure 23. Valve mounted on alignment testbed.

V. Conclusion

Temperature sensitive paint was used to visualize stationary crossflow vortices on a 7° cone at 6° angle of attack. Small roughness was added near the nosetip around the azimuth. Two tests were done to help determine if the applied roughness was generating the stationary vortices. First the cone was rolled approximately 10°, and the vortices rolled with the cone with both sets of roughness spacings. Second, the leading edge of the paint was moved much further downstream than in previous tests in order to lessen any effect that the paint edge and the painted surface has on the generation of stationary vortices. When the spacing of the roughness was altered, the spacing of the stationary vortices was also altered. Therefore it appears that the roughness elements are dominating the generation of the stationary vortices.

The pulsed jet perturber saw improved performance as a result of modifications to the circuit driving the valve. Pulse duration was reduced from approximately 800–1000μs to 300–500μs when compared with previous testing. Further refinement is required in the alignment procedure to allow for more consistent performance from run to run. This will be accomplished via the newly built alignment test bed. Additional system modifications are being investigated in an effort to further reduce the pulse duration. Low-frequency disturbances in the predicted first-mode instability frequency range were measured on the surface of a cone-ogive-cylinder model in the BAM6QT. However, the peak disturbance frequency did not change with total pressure as predicted by computations. Additionally, since entropy-layer instabilities have a similar frequency range as the first-mode instability, experimental measurements off the model surface are being taken to determine if the measured low-frequency disturbance is an entropy-layer instability. Initial measurements show that the magnitude of the low-frequency disturbance on the cone-ogive-cylinder is greatest outside the boundary layer which may indicate an entropy-layer instability. Additional experiments and analysis is required to better classify these measured disturbances.

VI. Acknowledgements

The authors would like to thank the Air Force Office of Scientific Research for their funding under grant number FA9550-12-1-0167, and Heath Johnson and Graham Candler at the University of Minnesota for installing STABL on our Purdue computer and for their assistance in running the code. Abney would also like to thank Sandia National Laboratories for partial support.

References

[1]Tirtey, S. C., *Characterization of a Transitional Hypersonic Boundary Layer in Wind Tunnel and Flight Conditions*, Ph.D. thesis, Von Karman Institute for Fluid Dynamics, Brussels, Belgium, August 2006.

[2]Morkovin, M., "Critical Evaluation of Transition from Laminar to Turbulent Shear Layers with Emphasis on Hypersonically Travelling Bodies," Air Force Flight Dynamics Laboratory Rep. AFFDL-TR-68-149, April 1969.

[3]Reed, H., Saric, W., and Arnal, D., "Linear Stability Theory Applied to Boundary Layers," *Annual Review of Fluid Mechanics*, Vol. 28, 1996, pp. 389–428.

[4]Saric, W., Reed, H., and White, E., "Stability and Transition of Three-Dimensional Boundary Layers," *Annual Review of Fluid Mechanics*, Vol. 35, 2003, pp. 413–440.

[5]Deyhle, H. and Bippes, H., "Disturbance Growth in an Unstable Three-Dimensional Boundary Layer and its Dependence on Environmental Conditions," *Journal of Fluid Mechanics*, Vol. 316, December 1996, pp. 73–113.

[6]Saric, W. S., Jr., R. B. C., and Reibert, M. S., "Nonlinear Stability and Transition in 3-D Boundary Layers," *Meccanica*, Vol. 33, 1998, pp. 469–487.

[7]Corke, T., Matlis, E., Schuele, C.-Y., Wilkinson, S., Owens, L., and Balakumar, P., "Control of Stationary Cross-flow Modes Using Patterned Roughness at Mach 3.5," *7th IUTAM Symposium on Laminar-Turbulent Transition*, 2010, pp. 123–128.

[8]Schuele, C. Y., *Control of Stationary Cross-Flow Modes in a Mach 3.5 Boundary Layer Using Patterned Passive and Active Roughness*, Ph.D. thesis, University of Notre Dame, South Bend, Indiana, December 2011.

[9]Chou, A., Ward, C. A. C., Letterman, L. E., Luersen, R. P. K., Borg, M. P., and Schneider, S. P., "Transition Research with Temperature-Sensitive Paints in the Boeing/AFOSR Mach-6 Quiet Tunnel," AIAA Paper 2011-3872, June 2011.

[10]Li, F., Choudhari, M., Chang, C.-L., and White, J., "Analysis of Instabilities in Non-Axisymmetric Hypersonic Boundary Layers over Cones," AIAA Paper 2010-4643, June 2010.

[11]Abney, A., Ward, C., Berridge, D., Greenwood, R., and Schneider, S. P., "Hypersonic Boundary-Layer Transition Experiments in the Boeing/AFOSR Mach-6 Quiet Tunnel," AIAA Paper 2013-0375, January 2013.

[12]Alba, C. R., Casper, K. M., Beresh, S. J., and Schneider, S. P., "Comparison of Experimentally Measured and Computed Second-Mode Disturbances in Hypersonic Boundary-Layers," AIAA Paper 2010-0897, January 2010.

[13]Estorf, M., Radespiel, R., Schneider, S. P., Johnson, H. B., and Hein, S., "Surface-Pressure Measurements of Second-Mode Instability in Quiet Hypersonic Flow," AIAA Paper 2008-1153, January 2008.

[14]Chang, C.-L., Choudhari, M. M., Hollis, B. R., and Li, F., "Transition Analysis for the Mars Science Laboratory Entry Vehicle," AIAA Paper 2009-4076, June 2009.

[15]Demetriades, A., "Hypersonic Viscous Flow over a Slender Cone, Part III: Laminar Instability and Transition," AIAA Paper 1974-0535, June 1974.

[16]Demetriades, A., "Growth of disturbances in a laminar boundary layer at Mach 3," *Phys. Fluids A*, Vol. 1, No. 2, 1989, pp. 312–317.

[17]Kendall, J. M., "Wind Tunnel Experiments Relating to Supersonic and Hypersonic Boundary-Layer Transition," *AIAA Journal*, Vol. 13, No. 3, 1974, pp. 290–299.

[18]N. S. Dougherty, J. and Fisher, D. F., "Boundary Layer Transition on a 10-Degree Cone: Wind Tunnel/Flight Data Correlation," AIAA Paper 1980-0154, January 1980.

[19]N. Sam Dougherty, J. and Fisher, D. F., "Boundary-Layer Transition Correlation on a Slender Cone in Wind Tunnels and Flight for Indications of Flow Quality," Tech. Rep. Final Report for Period January 1970 to November 1978, AEDC-TR-81-26, 1982.

[20]Stetson, K. F., Thompson, E. R., Donaldson, J. C., and Siler, L. G., "Laminar Boundary Layer Stability Experiments on a Cone at Mach 8, Part 1: Sharp Cone," AIAA Paper 1983-1761, July 1983.

[21]Stetson, K. F., Thompson, E. R., Donaldson, J. C., and Siler, L. G., "A Comparison of Planar and Conical Boundary Layer Stability and Transition at a Mach Number of 8," AIAA Paper 1991-1639, June 1991.

[22]Stetson, K. F. and Kimmel, R. L., "On Hypersonic Boundary-Layer Stability," AIAA Paper 1992-0737, January 1992.

[23]Munoz, F., Heitmann, D., and Radespiel, R., "Instability Modes in Boundary Layers of an Inclined Cone at Mach 6," AIAA Paper 2012-2823, June 2012.

[24]Stetson, K. F., Thompson, E. R., Donaldson, J. C., and Siler, L. G., "Laminar Boundary Layer Stability Experiments on a Cone at Mach 8, Part 2: Blunt Cone," AIAA Paper 1984-0006, January 1984.

[25]Reshotko, E. and Khan, M. M. S., "Stability of the Laminar Boundary Layer on a Blunted Plate in Supersonic Flow," Springer-Verlag, Stuttgart, Germany, September 1980, pp. 186–200.

[26]Johnson, H. B., "Stability and Transition Analysis for Hypersonic Boundary Layers Program Reference," University of Minnesota Unpublished Report, April 2010.

[27]Johnson, H. B. and Candler, G. V., "Hypersonic Boundary Layer Stability Analysis Using PSE-Chem," AIAA Paper 2005-5023, June 2005.

[28]Berridge, D. C., *Measurements of Second-Mode Instability Waves in Hypersonic Boundary Layers with a High-Frequency Pressure Transducer*, Master's thesis, Department of Aeronautics and Astronautics, Purdue University, West Lafayette, IN, December 2010.

[29]Wright, R. and Zoby, E., "Flight Boundary Layer Transition Measurements on a Slender Cone at Mach 20," AIAA Paper 77-719, June 1977.

[30]Krishnan, L. and Sandham, N., "On the merging of turbulent spots in a supersonic boundary-layer flow," *International Journal of Heat and Fluid Flow*, Vol. 27, 2006, pp. 542–550.

[31]Makita, H. and Nishizawa, A., "Characteristics of internal vortical structures in a merged turbulent spot," *Journal of Turbulence*, July 2001.

[32]Park, S. and Lauchle, G. C., "Wall pressure fluctuation spectra due to boundary-layer transition," *Journal of Sound and Vibration*, Vol. 319, 2009, pp. 1067–1082.

[33]Casper, K., Beresh, S., and Schneider, S., "Spanwise Growth of the Turbulent Spot Pressure-Fluctuation Field in a Hypersonic Boundary Layer," AIAA Paper 2011-3873, June 2011.

[34]Casper, K. M., *Pressure Fluctuations Beneath Instability Wave Packets and Turbulent Spots in a Hypersonic Boundary Layer*, Ph.D. thesis, Purdue University, August 2012.

[35]Ching, C. Y. and LaGraff, J. E., "Measurements of turbulent spot convection rates in a transitional boundary layer," *Experimental Thermal and Fluid Science*, Vol. 11, 1995, pp. 52–60.